Supplement of Atmos. Meas. Tech., 18, 7053–7073, 2025
https://doi.org/10.5194/amt-18-7053-2025-supplement

Atmospheric Measurement Techniques
Open Access

Supplement of

If the Yedoma thaws, will we notice? Quantifying detection limits of top-down methane monitoring infrastructures

Martijn M. T. A. Pallandt et al.

Correspondence to: Martijn M. T. A. Pallandt (martijn.pallandt@natgeo.su.se)

S1 Station information

Site	Site code	Latitude	Longitude	Elevation	Inlet Height	Network	Region
Ambarchik	AMB	69.62	162.30	20	27	MPI-BGC	Siberia
Barrow	BRW	71.32	-156.61	11	16	NOAA	Alaska
Tiksi	TIK	71.60	128.89	19	10	FMI	Siberia
Tiksi Flask	TIF	71.60	128.89	19	10	NOAA	Siberia
Kjolnes	KJN	70.85	29.24	1	4	Uni-Exeter	Europe
Zeppelin	ZEP	78.90	11.88	474	16	NILU	Europe
Alert	ALT	82.45	-62.51	200	10	EC	Canada
ZOTTO	ZOT	60.80	89.35	114	301	MPI-BGC	Siberia
Inuvik	INK	68.32	-133.53	113	10	EC	Canada
Behchoko	BCK	62.80	-115.92	160	60	EC	Canada
Cambridge Bay	CBY	69.13	-105.06	35	12	EC	Canada
CARVE Tower Fairbanks	CRV	64.99	-147.60	611	32	CARVE	Alaska
Baranov	BAR	79.28	101.62	20	10	FMI	Siberia
Dikson preliminary	DIP	73.50	80.40	15	20	Krasnoyarsk	Siberia
Pleistocene park	CHS	68.51	161.53	10	34	NOAA	Siberia
Pallas	PAL	67.97	24.12	560	20	FMI	Europe
Abbotsford	ABT	49.01	-122.34	60	33	EC	Canada
Bratts_Lake	BRA	50.20	-104.71	595	35	EC	Canada
Candle_Lake	CDL	53.99	-105.12	600	30	EC	Canada
Chapais	CPS	49.82	-74.98	391	8; 40	EC	Canada
Chibougamau	CHB	49.69	-74.34	393	30	EC	Canada
Churchill	CHL	58.74	-93.82	29	60	EC	Canada
East_Trout_Lake	ETL	54.35	-104.99	493	105	EC	Canada
Egbert	EGB	44.23	-79.78	251	3; 25	EC	Canada
Estevan_Point	ESP	49.38	-126.54	7	40	EC	Canada
Esther	EST	51.67	-110.21	707	3; 50	EC	Canada
Fort_Nelson	FNE	58.84	-122.57	361	15	EC	Canada
Fraserdale	FSD	49.88	-81.57	210	40	EC	Canada
Hanlans_Point	HNP	43.61	-79.39	87	10	EC	Canada
Lac_La_Biche	LLB	54.95	-112.47	540	10; 50	EC	Canada
Sable_Island	WSA	43.93	-60.01	5	25	EC	Canada
Toronto	TAO	43.66	-79.40	110	174	EC	Canada
Turkey_Point	TKP	42.64	-80.55	231	35	EC	Canada
Berezorechka	BRZ	56.15	84.33	168	5; 20; 40; 80	JR-STATION	Siberia
Karasevoe	KRS	58.25	82.42	76	35; 67	JR-STATION	Siberia
Igrim	IGR	63.19	64.41	9	24; 47	JR-STATION	Siberia
Noyabrsk	NOY	63.43	75.78	108	21; 43	JR-STATION	Siberia
Demyanskoe	DEM	59.79	70.87	63	45; 63	JR-STATION	Siberia
Savvushka	SVV	51.33	82.13	495	27; 52	JR-STATION	Siberia
Azovo	AZV	54.71	73.03	110	29; 50	JR-STATION	Siberia
Vaganovo	VGN	54.50	62.32	192	42; 85	JR-STATION	Siberia
Yakutsk	YAK	62.09	129.36	264	11; 77	JR-STATION	Siberia
Cold Bay	CBA	55.21	-162.72	21.34	NA	NOAA	Alaska
Storhovdi Island	ICE	63.40	-20.29	118	9	NOAA	Europe
Mace Head	MHD	53.33	-9.90	5	NA	NOAA	Europe
Shemya Island	SHM	52.71	174.13	23	NA	NOAA	Alaska
Summit	SUM	72.60	-38.42	3210	5	NOAA	Europe
SMEAR II-ICOS Hyytiaelae	ATM-HYY	61.85	24.29	183	125	ICOS	Europe
Sodankylae GAW station	SOD	67.36	26.64	179	48	ICOS	Europe
Puijo-Koli ICOS	ATM-PUI	62.91	27.66	230	85	ICOS	Europe
ICOS Utoe - Baltic sea	ATM-UTOE	59.78	21.37	8	56	ICOS	Europe
Station Nord	SNO	81.60	-16.66	24	NA	ICOS	Europe
Station Nord first coordinates	SN1	81.60	-16.66	24	80	ICOS	Europe
Station Nord Preliminary	DK-SNP	81.36	-16.39	24	80	ICOS	Europe
Birkenes Observatory	BIR	58.38	8.25	190	NA	ICOS	Europe
Svartberget	SVB	64.26	19.77	267	150	ICOS	Europe

Norunda	NOR	60.09	17.48	46	101	ICOS	Europe
Hyltemossa	HYL	56.10	13.42	115	148	ICOS	Europe
Teriberka	TER	69.20	35.10	40	2	MGO	Russia
Baker Lake	BLK	64.33	-96.01	95	10	EC	Canada
Downsview	DWN	43.78	-79.47	198	20	EC	Canada
Fort McKay South	FMS	57.19	-111.64	250	10	EC	Canada
Mould Bay	MBC	76.25	-119.35	30	NA	EC	Canada

Table S1: Tower network, indicating: site name, site code, latitude, longitude, ground elevation above sea level in meters, inlet height(s) in meters, associated network, and region.

S2 TROPOMI Uncertainty fit

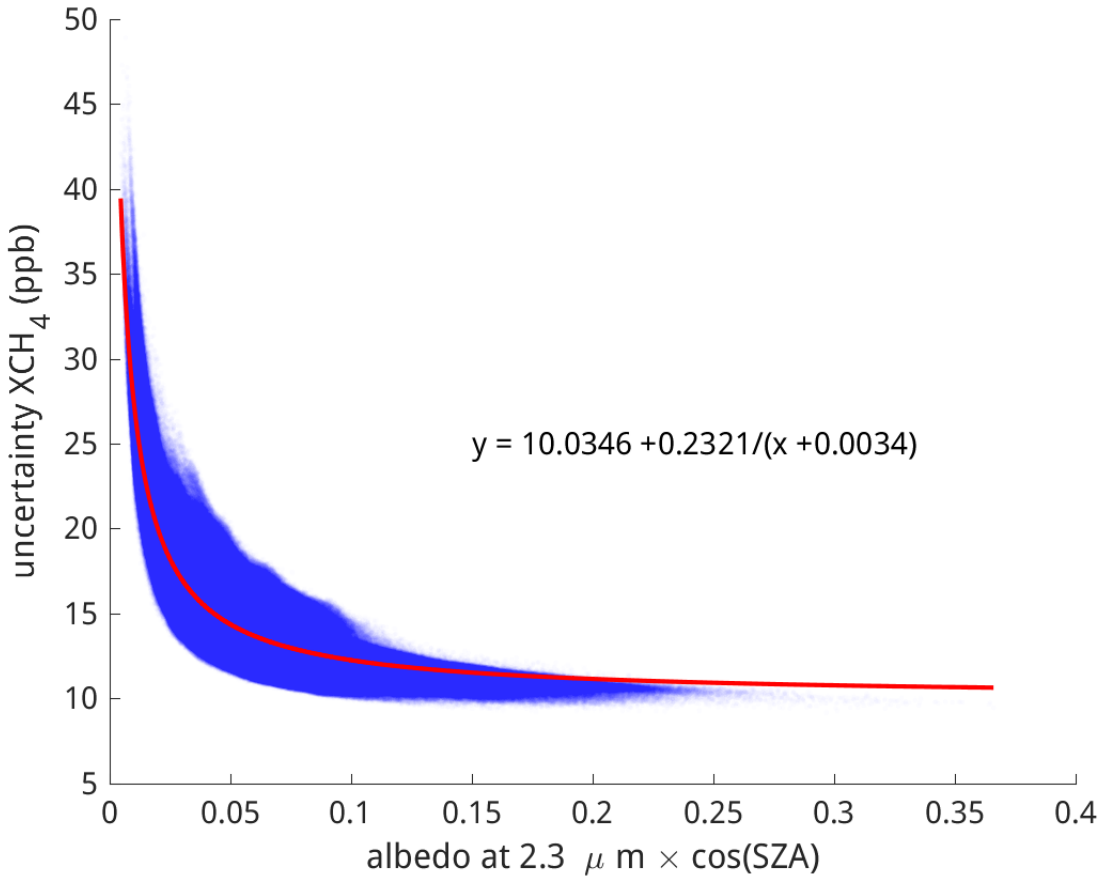

Figure S1: The reported measurement error of every fifth good sounding north of 50 °N from the WFMD V2.0 XCH_4 product from the years 2020–2021, plotted against the product of the retrieved albedo at 2.3 µm and the cosine of the solar zenith angle (SZA). The red line shows the function fit to the curve, given by Equation 1.

S3 Averaging Kernels

Because the shape of the averaging kernel depends on the characteristics of the retrieval itself, in addition to factors like the temperature, water vapour profile, and viewing geometry, it is difficult to generalize it for the production of synthetic observations. Calculations with a standard atmosphere show only a slight dependence on the SZA, and a generally flat shape from the surface to about 200 hPa, above which it drops off slightly (c.f. Figure 2 in Schneising et al. (2019). This is confirmed when averaging all good soundings north of 50°N for the year 2020 by SZA, as shown in Figure S2. The mean is shown as a solid line, and the shaded area represents one standard deviation around the mean.

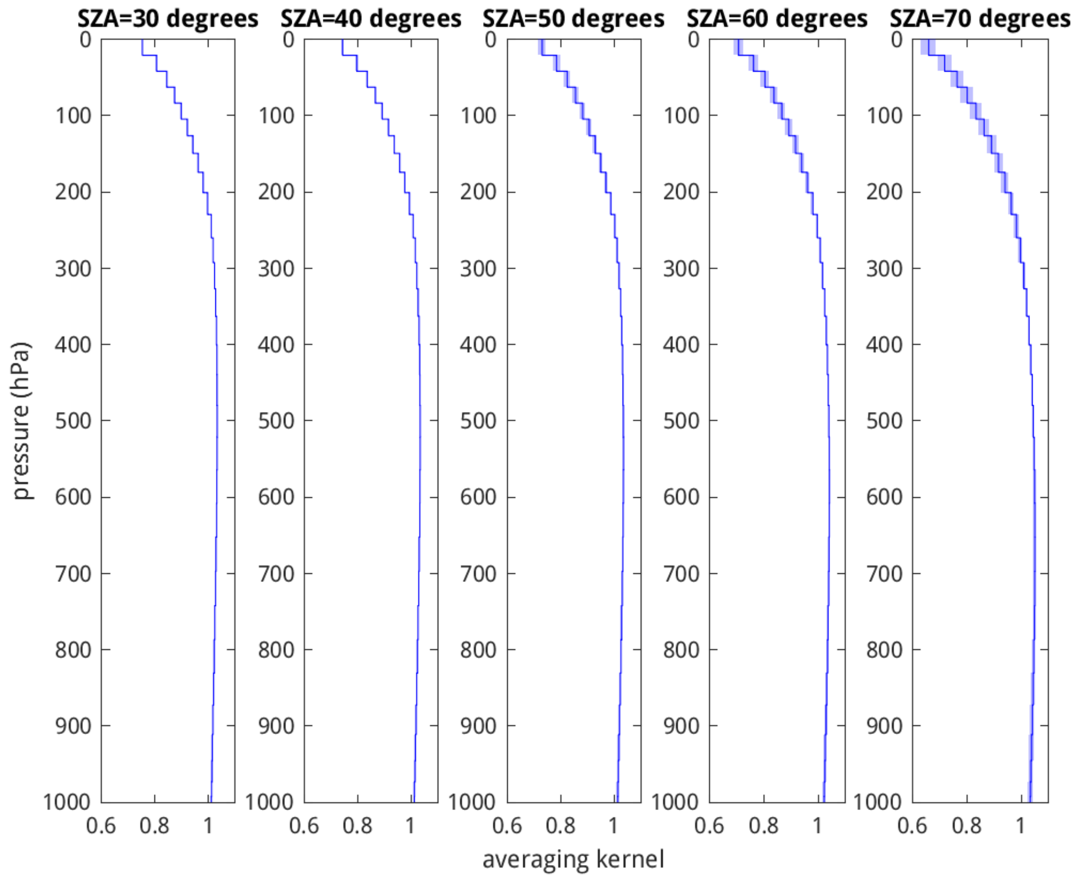

Figure S2: The mean averaging kernel per SZA bin (where the 30°bin includes all soundings with 25°≤ SZA < 35°, and so on), with the standard deviation shown as a shaded area per level. This is based on all good WFMD XCH4 soundings above 50°N for the year 2020. In practice, the vertical axis shifts with the surface pressure. Here the mean pressure weight for each of the 31 layers is shown for a surface pressure of 1000 hPa.

To compare the effective vertical weighting of the TROPOMI soundings with those of MERLIN, an example weighting function for a surface pressure of 1000 hPa as used in Bousquet et al. (2018) was considered. To make the averaging kernel comparable with the weighting function of MERLIN, a weight per layer was calculated by multiplying the mean averaging kernel of TROPOMI with the pressure thickness of each layer after first interpolating the 31-level averaging kernel of TROPOMI onto the 19 levels of the MERLIN weighting function. Likewise, a flat, pressure-weighted averaging kernel was considered, where the weight is simply the pressure thickness of each layer divided by the surface pressure. The result can be seen in Figure S3. Based on the similarity of these curves, the choice of a pressure-weighted column averaging for both the MERLIN and the TROPOMI synthetic measurements seems acceptable. The sensitivity of MERLIN to near-surface signals may be slightly underestimated compared, but for TROPOMI the estimate is quite close.

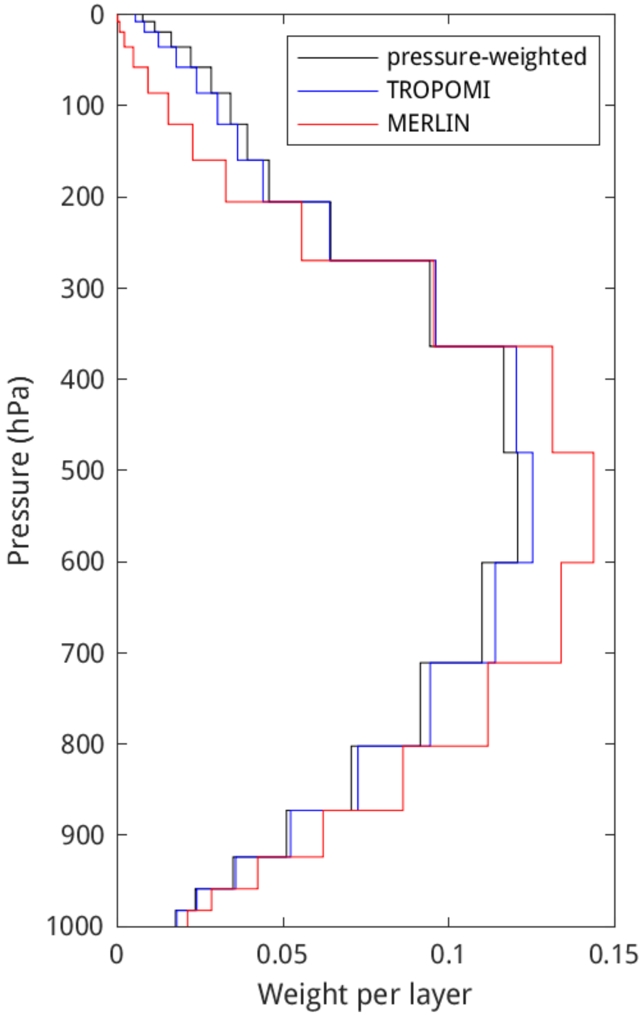

Figure S3. The weighting function for MERLIN (red), TROPOMI (blue) and a flat averaging kernel (black) for each of the 19 vertical layers of the example MERLIN weighting function. The weighting function for TROPOMI is derived by multiplying the averaging kernel value (interpolated onto the same pressure axis) with the pressure weight of each layer. All three curves sum up to 1.0.

S4 Minimal detection limits

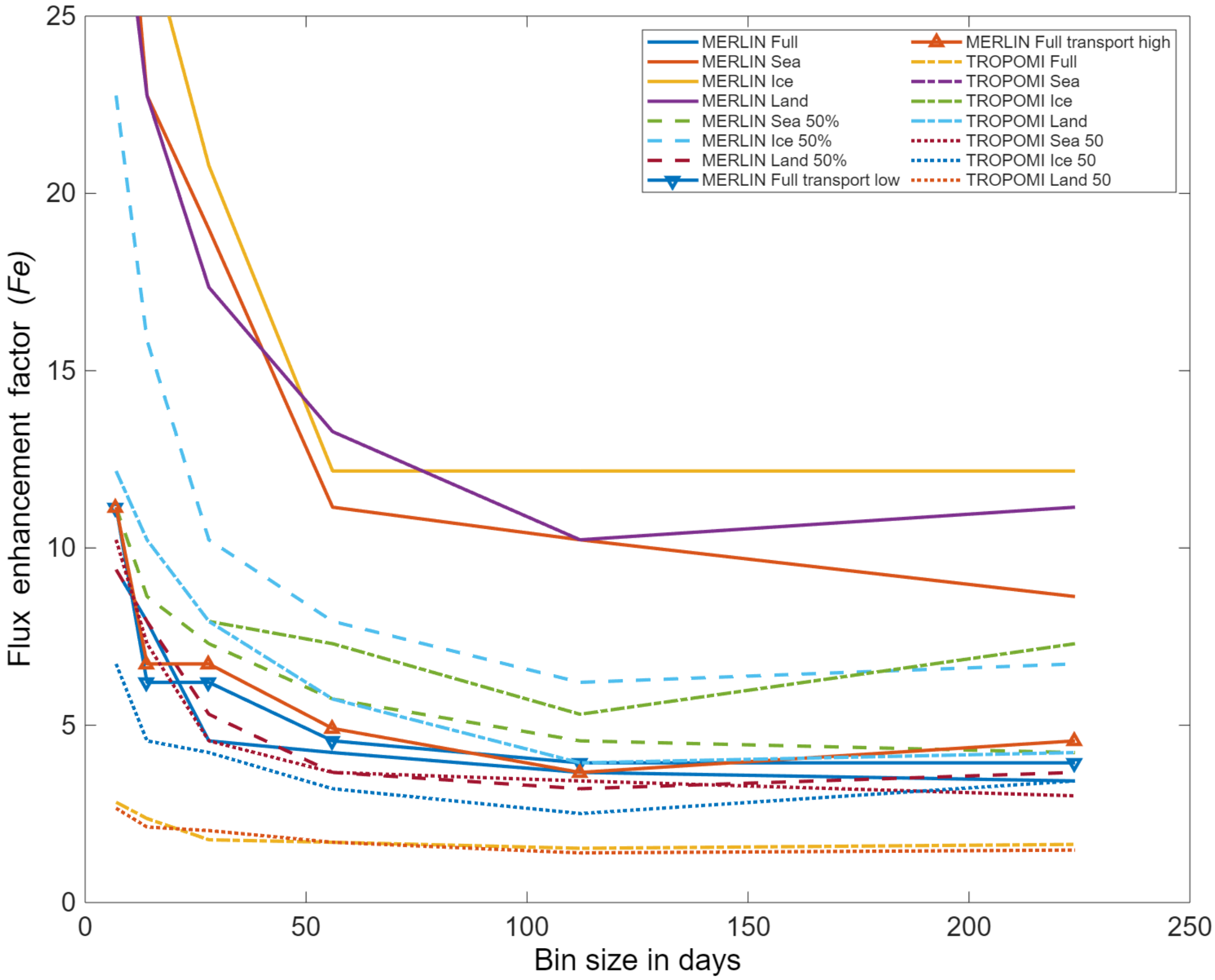

Figure S4: Minimal detection limits for MERLIN and TROPOMI by temporal bin size. The Y-axis shows the Fe values of the lowest detection limits (note the shorter Y-axis and linear scale). On the X-axis the size of temporal bins is given. Solid lines for the respective MERLIN cases. Dashed lines for MERLIN cases of which the pixels selected matches at least half the qualifier. Solid lines with triangle indicate the Full MERLIN case with the addition of transport modelling errors. Dash dotted lines for the respective TROPOMI cases. Dotted lines for MERLIN cases of which the pixels selected matches at least half the qualifier. We see optimal detection limits at a temporal bin size of 112 days. More details on these cases in Table 1 and sections 2.3 and 2.4.